Improved interpretability from elastic full waveform inversion model-based seismic images revitalizes Paleogene development in the Gulf of Mexico

Abhijit Gangopadhyay[1], Li Jiang[1], Robert Chrisman[1], Sanjay Banerjee[1], Han Su[2], Bin Deng[2], Bharat Bonala[2], Jiawei Mei[2]*

[1]*bp*
[2]*Viridien*

Summary

We present a case study of reimaging the subsalt Paleogene reservoirs in a field in the Gulf of Mexico using an elastic full waveform inversion based velocity model. Compared to the legacy images, the results of this campaign show better definition of the salt weld geometry, visibility of its internal structure, clarity of the container boundaries, and granularity within the target reservoirs. All these improvements aid interpretation of the target reservoirs, which in turn results in better resource estimates, placement of future wells, and overall economic field development. This case study highlights the positive impact of advances in subsalt imaging on Paleogene field development in the Gulf of Mexico.

Introduction

The Wilcox (Paleogene) trend in the deepwater Gulf of Mexico (GOM) spans a vast area comprising Alaminos Canyon in the west, Keathley Canyon in the center, Walker Ridge in the east, and beyond (Chowdhury and Borton, 2007; Meyer et al., 2007). It contains Lower Eocene – Upper Paleocene reservoirs, which have been the focus of hydrocarbon exploration and appraisal activities since the beginning of the century (Meyer et al., 2007; Oletu et al., 2013). However, development of these reservoirs has faced significant challenges due to their rock properties, depth, overburden complexity, subsalt imaging quality, and engineering design and execution, amongst other reasons (Addison et al., 2010). Recent technological advances across disciplines have spurred rapid industry-wide growth in appraisal activities and final investment decisions for field development (Ait-Ettajer et al., 2017). Paramount among the advances are those in subsalt imaging, aided by better illumination (e.g., Lewis et al., 2016), increased data density, and use of acoustic and elastic FWI based velocity models and Imaging (e.g., Shen et al., 2017; Zhang et al., 2018; Wang et al., 2019; Zhang et al., 2020; Huang et al., 2021; van Gestel, 2021; Zhang et al., 2023). Herein, we describe a case from the deepwater GOM where imaging using elastic FWI has improved our interpretation of the Paleogene reservoirs in the Keathley Canyon area.

Background

bp's Paleogene portfolio dates to the mid-2000s and has since undergone various episodes of appraisal activities. Multidisciplinary technological breakthroughs and improved understanding of what makes subsalt Paleogene developments economical have resulted in renewed focus on these reservoirs in the GOM during the last decade. At the same time, recent successful applications of advances in subsalt seismic imaging within bp's Miocene portfolio in the GOM (Elebiju et al, 2022; Buist et al., 2023) brought the Paleogene to the forefront.

The Paleogene field that is the subject of our study faces several subsurface interpretation challenges arising from inadequate legacy seismic images. Figure 1 shows a seismic data quality map based on the average signal-to-noise ratio (S/N) at the target Paleogene reservoirs. Areas in red depict those where the seismic images are poor, and the distribution of these roughly align with that of the salt weld (e.g., Location 1 in Figure 1). The extent and geometry of this weld are not easily mappable, resulting in significant uncertainties in outlining the up-dip trap edge of the field, which in turn leads to wide ranges of resource estimates.

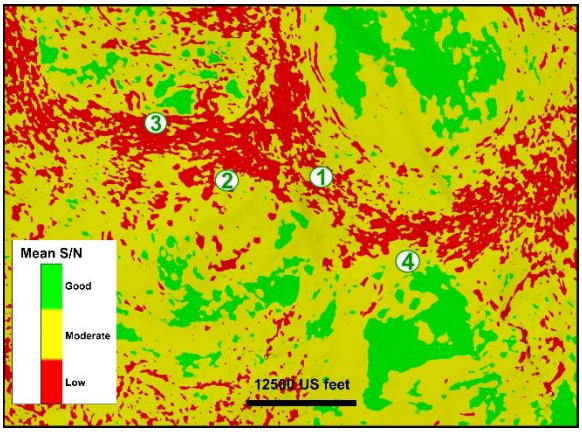

Figure 1: Seismic data quality map based on average S/N. 1 – 4 are representative areas of interpretation challenges described in the text.

The legacy images of the Paleocene reservoirs within the field are also challenged (e.g., Location 2 in Figure 1). The Paleocene interval exhibits low reflectivity compared to its immediate overburden (Figure 2), which adds to the difficulties in its interpretation. Across the field, the top of the Paleocene interval is somewhat mappable but not

unequivocally, particularly in the west (Figure 2). The west - northwestern limits of the field are unclear and cannot be mapped with confidence on the legacy data (Location 3 in Figure 1). Across the structure, relatively large faults that broadly define it are identifiable; however, smaller faults in the east are unclear (e.g., Location 4 in Figure 1), resulting in concerns about possible compartmentalization, which has the potential to negatively impact the economics of field development.

A seismic reprocessing campaign was therefore initiated in 2022 to build an elastic FWI-based velocity model and reimage the field. The data used to build the FWI-based velocity models are from the proprietary ocean bottom node (OBN) survey conducted over the field in 2021 and a long-offset, full-azimuth streamer survey acquired in 2012. Data from these surveys provide the necessary long offsets and full azimuthal coverage for FWI. Following the velocity model building, the reverse time migration (RTM) imaging workflow utilized data from the 2021 OBN survey and another proprietary wide-azimuth towed-streamer (WATS) survey conducted earlier over the field. The latter is used to provide adequate areal coverage in addition to the OBN patch. The velocity model building workflow is described next.

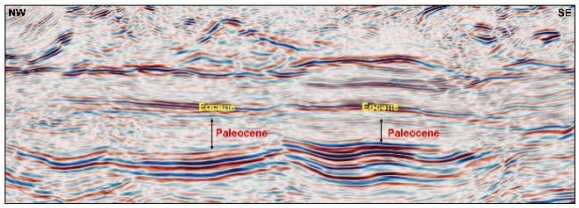

Figure 2: An example NW – SE seismic line on the legacy 18 Hz RTM image. The approximate locations of Eocene and Paleocene intervals (zone highlighted within the double-headed arrows) are shown. Of note is the overall low reflectivity in the Paleocene and the difficulty mapping its top in the west-northwest.

Methodology

To improve the imaging of the Paleogene, a velocity model building workflow driven by elastic Time-lag FWI (E-TLFWI) was adopted using the OBN and long-offset, full-azimuth streamer data. Beginning with the legacy model, one round of acoustic Time-lag FWI (A-TLFWI) up to 8 Hz was carried out to improve the model's overall kinematics, and thus build a better initial model for subsequent E-TLFWI applications. As shown in Figure 3, compared to the legacy velocity model, the 8 Hz A-TLFWI model provides a more geologically conformal update, with better delineated features, and rebuilds the overburden salt body (black arrows in Figures 3a and b). It also reveals a slow-velocity geobody that bounds the container edge (white arrows in Figures 3a and b). These velocity updates in the 8 Hz A-TLFWI model led to clear uplifts in the RTM image, with a better-defined container edge, improved continuity, and sharper focusing of the Paleogene events, which were difficult to map in the legacy image (yellow ellipses in Figures 3f and g). However, strong elastic effects, associated with large impedance contrasts, resulted in smeared boundaries of the salt body and container boundary in the acoustic FWI result, which consequently degraded the image and posed challenges for detailed reservoir mapping.

To mitigate these issues, E-TLFWI was applied on top of the A-TLFWI model to better account for the elastic effects. By integrating the elastic wave propagation engine with the time-lag cost function, E-TLFWI has proven to be a superior algorithm to A-TLFWI in explaining the recorded field data and updating the sediment-salt interface, thereby providing an improved velocity model and corresponding FWI-derived reflectivity (FDR) image, or the so-called FWI Image, with reduced smearing and better S/N, especially in the subsalt area (Wu et al., 2022; Zhang et al., 2023; Buist et al., 2023; Liu et al., 2023).

When compared to the 8 Hz A-TLFWI, the 8 Hz E-TLFWI model showed greatly reduced smearing around large-impedance contrasts, such as the salt halo (black arrows in Figures 3b and c). As a result, the salt body, the slow salt-exit velocity extension, and the slow geobody (white arrows in Figures 3b and c) were better delineated. In addition, the 8 Hz E-TLFWI model exhibited improved S/N along with enhanced velocity contrast. Consequently, the RTM image using the 8 Hz E-TLFWI model showed improved focusing and continuity of the reflectors near the salt body (cyan arrows in Figures 3g and h) and better imaging of the container edge (green arrows in Figures 3g and h).

Although the RTM images showed clear uplifts in the Paleogene from the legacy model to the A-TLFWI model, and then to the E-TLFWI model, the images in the area still had challenges due to inadequate S/N and limited illumination of the primary reflection energy throughout the complex overburden. To further improve the Paleogene image in this area, E-TLFWI was continued up to 15 Hz for FDR image derivation (Zhang, et al., 2020). This 15 Hz elastic FDR image (Figure 3i) better reveals the geologic features in the low-illumination zones and shows an improved S/N around the Paleogene because of the iterative least-squares data fitting of the full wavefield in FWI Imaging. However, the resolution of the 15 Hz elastic FDR image is still inadequate to reveal the desired details at the reservoir level. The E-TLFWI was therefore run up to 25 Hz. The final 25 Hz E-TLFWI velocity model, and the corresponding elastic FDR image (Figure 3j), show noticeable improvements in resolution. The container boundary, the structure around it, and the extent of the

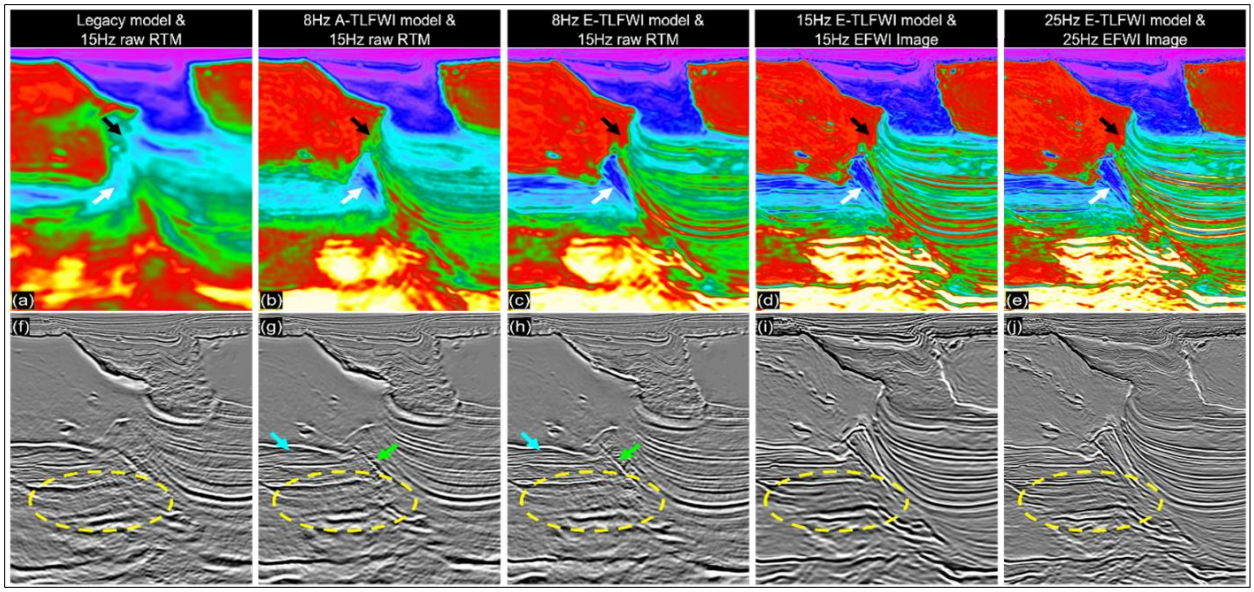

Figure 3: Velocity models and corresponding RTM and FDR images. (a) & (f) legacy model and 15 Hz OBN RTM, (b) & (g) 8 Hz A-TLFWI model and 15 Hz OBN RTM, (c) & (h) 8 Hz E-TLFWI model and 15 Hz OBN RTM, (d) & (i) 15 Hz E-TLFWI model and 15 Hz FDR image, (e) & (j) 25 Hz E-TLFWI model and 25 Hz FDR image.

Paleogene reflectors are further delineated, which benefit their mapping and interpretation.

Results

One of the easily observed improvements in the early elastic FDR images is the clear base of salt (Figure 4). In comparison to the acoustic FDR image, the ringing around the base of salt (Figure 4 – left) is eliminated in the elastic FDR image (Figure 4 – right).

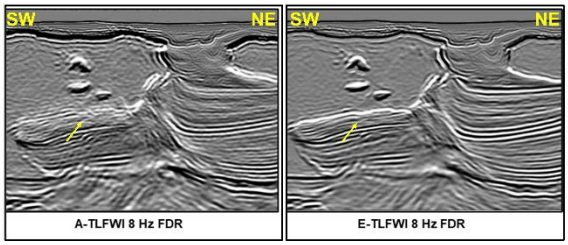

Figure 4: An example SW – NE seismic line from the 2022 reprocessing campaign showing an 8 Hz acoustic (left) and elastic (right) FDR image. The yellow arrows highlight the crisp base of salt (BOS) seen on the elastic FDR image (right) compared to the fuzzy one on the acoustic FDR image (left).

Figure 5 compares a legacy 15 Hz acoustic FDR image with a reprocessed elastic FDR image. On the latter, the extent of the salt weld and its internal character are clearer (dotted box in Figure 5). The terminations of the Eocene and Paleocene reflectors on either side of the weld are also sharper on the elastic FDR image and show more continuity and character compared to those on the acoustic FDR image (Figure 5).

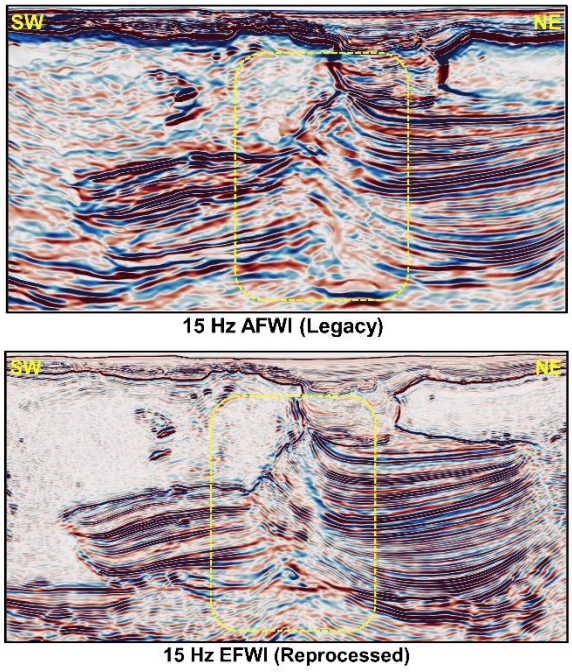

Figure 5: An example SW – NE seismic line showing a 15 Hz acoustic FDR image from the legacy data set (top) and a 15 Hz elastic FDR image from the 2022 reprocessing campaign (bottom). The dotted yellow box highlights the area around the salt weld wherein the elastic FWI-based image (bottom) shows significant improvements compared to the acoustic FDR image (top).

A traverse across the field allows for better interpretability of the transition from east to west on the elastic FDR image compared to that on the acoustic image (Figure 6). Additionally, the demarcation of the field boundary to the west is clearer on the elastic FDR image (Figure 6).

To better resolve the Paleocene interval, elastic FWI models with increasing frequencies (as much as the signal in the data allowed) are built. Figures 7 a-d demonstrate the impact of increasing frequencies on the resulting image. The higher frequencies reveal more character, possible geology within the Paleocene section, and additional features within the salt weld (Figures 7 a-d).

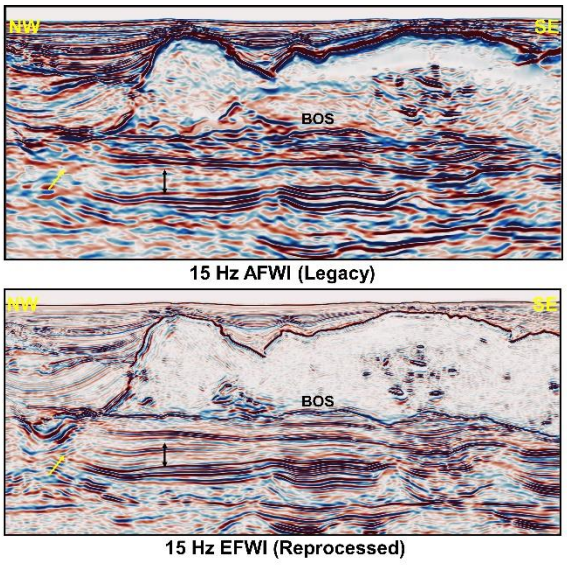

Figure 6: A NW – SE seismic line showing a legacy 15 Hz acoustic FDR image (top) and a 15 Hz elastic FDR image from the 2022 reprocessing campaign (bottom). The Paleocene interval approximately spans the double headed arrow on both the panels. The elastic FWI based image (bottom) shows a cleaner container boundary in the west (yellow arrow) and transition from the east to the west across the field, compared to the corresponding acoustic image.

Conclusions

In a subsalt environment, elastic FDR images have significantly better interpretability compared to their acoustic counterparts. The results discussed from this case

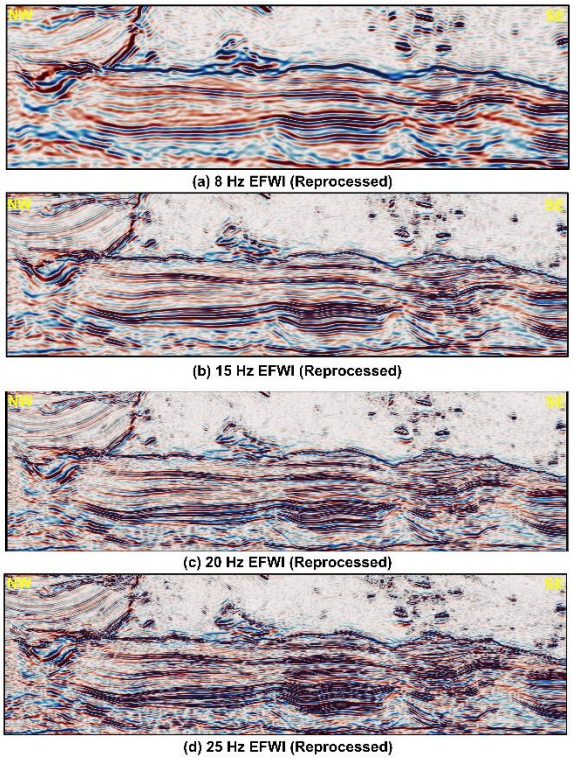

Figure 7: A representative NW – SE seismic line highlighting the impact of building elastic FWI models with increasing frequencies. The images here are from (a) 8 Hz (b) 15 Hz (c) 20 Hz and (d) 25 Hz elastic FWI models.

study of seismic imaging of a GOM Paleogene field demonstrate the above. The elastic FDR images outline the salt weld geometry better and show more of its internal structure. The field boundaries are clearer on the elastic FDR images. At higher frequencies, the Paleocene interval on the elastic FWI reveals more of the reservoirs and their continuity or lack thereof. A crisp base of salt on the elastic FDR image is a benefit to well planners as they chart out future well trajectories through the overburden. Overall, these improvements have resulted in less uncertain resource estimates, better future well placement capabilities, and economic field development scenarios. Together, once challenged subsalt Paleogene development in the GOM, is now rejuvenated, and advances in seismic imaging played an important part in it.

Acknowledgments

We thank bp and CGG for permission to publish this work.